

University of Massachusetts Amherst

From the Selected Works of Matthew Lackner

February, 2010

The Performance of Wind Turbine Smart Rotor Control Approaches During Extreme Loads

Matthew Lackner, *University of Massachusetts - Amherst*
Gijs A. M. van Kuik



Available at: https://works.bepress.com/matthew_lackner/2/

The Performance of Wind Turbine Smart Rotor Control Approaches During Extreme Loads

Matthew A. Lackner

Assistant Professor
Department of Mechanical and Industrial
Engineering,
University of Massachusetts Amherst,
160 Governors Drive,
Amherst, MA 01003
e-mail: lackner@ecs.umass.edu

Gijs A. M. van Kuik

Professor
Faculty of Aerospace Engineering,
Delft University Wind Energy Research Institute,
Kluyverweg 1,
2629 HS Delft, The Netherlands
e-mail: g.a.m.vankuik@tudelft.nl

Reducing the loads experienced by wind turbine rotor blades can lower the cost of energy of wind turbines. "Smart rotor control" concepts have emerged as a solution to reduce fatigue loads on wind turbines. In this approach, aerodynamic load control devices are distributed along the span of the blade, and through a combination of sensing, control, and actuation, these devices dynamically control the blade loads. While smart rotor control approaches are primarily focused on fatigue load reductions, extreme loads on the blades may also be critical in determining the lifetime of components, and the ability to reduce these loads as well would be a welcome property of any smart rotor control approach. This research investigates the extreme load reduction potential of smart rotor control devices, namely, trailing edge flaps, in the operation of a 5 MW wind turbine. The controller utilized in these simulations is designed explicitly for fatigue load reductions; nevertheless its effectiveness during extreme loads is assessed. Simple step functions in the wind are used to approximate gusts and investigate the performance of two load reduction methods: individual flap control and individual pitch control. Both local and global gusts are simulated. The results yield important insight into the control approach that is utilized, and also into the differences between using individual pitch control and trailing edge flaps for extreme load reductions. Finally, the limitation of the assumption of quasisteady aerodynamic behavior is assessed. [DOI: 10.1115/1.4000352]

1 Introduction

Wind turbines are subjected to significant and rapid fluctuating loads, which arise from a variety of sources including turbulence in the wind, tower shadow, wind shear, yawed flow, and gusts. Fatigue loads can lead to damage of turbine components and eventually to failures. "Smart rotor control" concepts have emerged as a possible means to reduce fatigue loads on wind turbines. In this approach, aerodynamic load control devices are distributed along the span of the blade, and through a combination of sensing, control, and actuation, these devices dynamically control the loads on the blades, at any azimuthal position. Previous research presented by the authors has focused on utilizing smart rotor control approaches for reducing blade fatigue loads [1].

The research presented here focuses on a distinct, but complementary problem: The potential to utilize smart rotor control approaches for reducing extreme loads due to gusts and safety system situations. While the reduction in fatigue loads is the primary objective of smart rotor control approaches such as individual pitch control (IPC) and individual flap control (IFC), the ability to reduce the damage due to extreme loads could be an important secondary property of any approach. Both fatigue loads and extreme loads contribute to the accrued damage in turbine components that eventually leads to failures. Load control devices and smart rotor control approaches that can reduce both types of loads may be especially advantageous and lead to significantly increased lifetimes of components or reduced costs.

This research investigates the issue of extreme loads by simulating the operation of a 5 MW turbine equipped with trailing edge flaps in an aero-elastic design code, GH BLADED. The load reduction controller utilized in this research, used for both IFC and IPC, is developed with the specific goal of reducing the blade fatigue loads. Since fatigue load reduction is the primary goal of the smart rotor approach, not surprisingly the controller is designed with

this goal in mind. On the other hand, these same load reduction controllers may operate under extreme situations as well. Thus, the performance of these smart control approaches, designed for fatigue load reductions, is assessed when extreme events occur.

1.1 Previous Work. Smart rotor control has become an active area of research for wind turbine applications [2]. Barlas and van Kuik [3] provided detailed summaries of smart rotor control research for wind turbines, including thorough reviews of potential actuators, sensors, aerodynamic control surfaces, control approaches, and simulation environments.

Individual pitch control is a popular potential smart rotor control concept, and several investigations into the use of IPC schemes have been conducted recently. van Engelen and van der Hooft [4], Bossayni [5], Selvam [6], along with others, have investigated control approaches for IPC, simulated IPC schemes, and demonstrated sizable load reduction capabilities of the IPC approach.

Smart rotor control simulations that utilize localized load control devices have also been conducted. In particular, the work of Andersen et al. [7], and McCoy and Griffin [8] simulate spanwise distributed load control devices, and provide a useful comparison to this research. The authors also investigate the use of smart rotor control for fatigue load reductions [1,9]. Other similar research includes the work of Zayas et al. [10]. In general, these investigations focus exclusively on fatigue loads during turbulent wind simulations, and not on extreme loads.

2 Modeling and Procedure

2.1 Turbine Model and Simulation Environment. The simulation of a 5 MW wind turbine with controllable trailing edge flaps is carried out using the aero-elastic simulation package GH BLADED [11,12]. Some of the important features that BLADED provides are as follows.

- Aerodynamics are calculated using the well-known blade element-momentum (BEM) approach. Dynamic inflow and dynamic stall models are also incorporated to model the

Contributed by the Solar Energy Division of ASME for publication in the JOURNAL OF SOLAR ENERGY ENGINEERING. Manuscript received November 3, 2008; final manuscript received July 27, 2009; published online December 21, 2009. Assoc. Editor: Spyros Voutsinas.

turbine wake and deal with unsteady aerodynamic conditions.

- The structural dynamics of the turbine model are calculated using a limited degree of freedom modal model.
- The dynamics of the power train (shaft, gearbox, and generator) are modeled.
- The external wind conditions can be generated, including 3D turbulent wind fields, wind shear, tower shadow effects, and prescribed gusts.
- Control of the turbine can be accomplished using either the internal controller provided by BLADED, or external controllers written by the user can be incorporated.
- The loads on the various components of the turbine and the turbine performance are calculated.

The wind turbine model used for the analysis in BLADED is the NREL 5 MW (also referred to as the UpWind 5 MW) wind turbine [13]. The turbine is a horizontal axis, three bladed, upwind, variable speed, pitch controlled turbine, with a 126 m rotor diameter, 90 m hub height, and 20 m water depth.

BLADED is capable of including trailing edge flaps (TEFs) in the turbine model, and allows the TEFs to operate concurrently with variable speed and pitch controlled operation. The TEFs are added to the blade planform from 70% to 90% span. The TEFs are chosen to have a chordwise length of 10% and a deflection range of ± 10 deg. These dimensions and deflection ranges are chosen partially based on the work of Troldborg [14], who investigated the effectiveness of trailing edge flaps for a variety of configurations.

The aerodynamic performance of the TEFs is determined using XFOIL 6.9, which is a 2D viscous panel code [15]. XFOIL is used to generate the coefficients of lift, drag, and pitching moment as a function of angle of attack, for TEF deflection angles ranging from -10 deg to 10 deg in 1 deg increments. A Reynolds number of 6×10^6 is used for these calculations.

For this research, in all sections on the blade, including the TEF sections, BLADED assumes quasisteady aerodynamic behavior and uses 2D airfoil table interpolation to determine the coefficients of lift, drag, and pitching moment. Thus, no dynamic stall model is utilized, and all behaviors are assumed to be quasisteady. This assumption is examined in detail below. A dynamic inflow model is still used in the BLADED simulations, but this model is not adapted for the TEF sections.

2.2 Turbine Control. External controllers, written in FORTRAN and compiled as .dll files, are used to control the wind turbine model in BLADED. These external controllers control the generator torque, blade pitch, and TEF deployment angles.

2.2.1 Standard Control. A baseline controller for the wind turbine model is provided by NREL. This is the “standard controller” for the NREL/UpWind 5 MW turbine model, and so it controls the generator torque and collective blade pitch, but does not control the TEFs. The generator torque control is a quadratic function of the generator speed in region 2 for optimal tip speed ratio operation. In region 3, the generator torque is used to produce constant power output of the turbine. The collective blade pitch is also used to control the rotor speed in region 3, with a basic gain scheduled proportional-integral-derivative (PID) controller.

2.2.2 Load Reduction Controller Design. A load reduction controller, used for both IFC and IPC, is developed with the specific goal of reducing the fatigue loads. As stated above, while this research is concerned with extreme loads due to gusts and transients, the control approach that is developed for reducing fatigue loads is not changed. Thus, the fatigue load reduction controller is now described, and is utilized throughout the simulations presented in this paper.

Similar challenges are faced when implementing IFC or IPC schemes, and similar solutions are needed. In fact, the structure of

the control approach for IFC and IPC is identical, and the only differences are the gains and the switching logic. A general “load reduction controller” is described first.

The load reduction controller requires additional control action compared with the standard controller in order to reduce the loads on the blades. In this approach, the standard controller logic remains unchanged, and so the generator torque and the collective blade pitch are controlled in an identical manner, while simultaneously the load control action, either deployment of the TEFs or the individual blade pitch, is performed independently.

Broadly, the goal of the load reduction control approach is to affect the blade root flapwise bending moment of each of the three blades (M_{y1} , M_{y2} , and M_{y3}), by adjusting either the TEFs or the blade pitch angles. This is a feedback control approach, and so the TEFs or blade pitch are changed based on measurements of M_{y1} , M_{y2} , and M_{y3} . The major challenge in implementing this feedback control approach is due to the fact that the blades are in a rotating coordinate system, and so the equations of motion that relate M_{y1} , M_{y2} , and M_{y3} and the TEFs or blade pitch contain periodic coefficients. The result is a linear time varying (LTV) system.

The issue of a rotating coordinate system has been identified numerous times in smart rotor control research [4–6,8,16]. The most common solution is a multiblade transformation, or Coleman transformation, which maps the individual blade variables in the rotating frame of reference into a fixed reference frame [17]. While it is not precisely true, it can be assumed that the transformed system is time invariant and so LTI control techniques can be used [4,6,16].

The Coleman matrix P and its inverse P^{-1} for a three bladed wind turbine are shown in Eqs. (1) and (2), respectively, where $\psi(t)$ is the azimuthal angle for each blade, and $\psi(t)=0$ occurs when a blade is positioned vertically upwards. P^{-1} is used to transform variables in the rotating frame of reference into the fixed frame, and P transforms variables from the fixed frame of reference into the rotating frame. The variables in the fixed and rotating coordinate systems are related according to

$$\begin{bmatrix} \theta_1(t) \\ \theta_2(t) \\ \theta_3(t) \end{bmatrix} = \begin{bmatrix} 1 & \sin \psi_1(t) & \cos \psi_1(t) \\ 1 & \sin \psi_2(t) & \cos \psi_2(t) \\ 1 & 2 \sin \psi_3(t) & \cos \psi_3(t) \end{bmatrix} \begin{bmatrix} \theta_1^{cm}(t) \\ \theta_2^{cm}(t) \\ \theta_3^{cm}(t) \end{bmatrix} \quad (1)$$

$$\begin{bmatrix} M_{y1}^{cm}(t) \\ M_{y2}^{cm}(t) \\ M_{y3}^{cm}(t) \end{bmatrix} = \frac{1}{3} \begin{bmatrix} 1 & 1 & 1 \\ 2 \sin \psi_1(t) & 2 \sin \psi_2(t) & 2 \sin \psi_3(t) \\ 2 \cos \psi_1(t) & 2 \cos \psi_2(t) & 2 \cos \psi_3(t) \end{bmatrix} \begin{bmatrix} M_{y1}(t) \\ M_{y2}(t) \\ M_{y3}(t) \end{bmatrix} \quad (2)$$

θ_1 , θ_2 , and θ_3 are either the TEF deployment angles or the pitch angles of each blade in rotating coordinates, and a superscript cm denotes variables in the fixed coordinate system. The variables in fixed coordinates are defined as follows.

- M_{y1}^{cm} is the average blade root flapwise bending moment, and as such is not a particularly useful variable.
- M_{y2}^{cm} is proportional to the yaw moment exerted by the blades on the fixed hub of the rotor.
- M_{y3}^{cm} is proportional to the tilt moment exerted by the blades on the fixed hub of the rotor.
- θ_{y1}^{cm} is the average, or collective, TEF deployment angle or blade pitch angle.
- θ_{y2}^{cm} is a differential TEF deployment angle or a differential pitch angle in the yaw-wise axis orthogonal to θ_{y3}^{cm} .
- θ_{y3}^{cm} is a differential TEF deployment angle or a differential pitch angle in the tiltwise axis orthogonal to θ_{y2}^{cm} .

θ_{y2}^{cm} and θ_{y3}^{cm} define how the three individual TEF angles or pitch angles vary from the collective angle [18]. It has been shown that the variables in the tiltwise axis and in the yaw-wise axis in the fixed coordinate system are nearly independent, and so the system

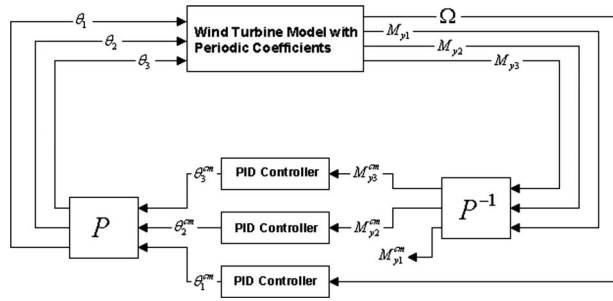


Fig. 1 Feedback control diagram for load reduction controller

can be decoupled into two independent, single input–single output (SISO) systems [4,5]. Specifically, θ_{y2}^{cm} directly controls the yaw-wise bending moment M_{y2}^{cm} , and θ_{y3}^{cm} directly controls the tiltwise bending moment M_{y3}^{cm} . Bossayni [5] pointed out that the assumption of independence between variables in the two axes is not entirely correct, but for this investigation the interaction between the axes is ignored for simplicity.

The collective TEF deployment angle or blade pitch angle θ_{y1}^{cm} directly controls the rotor speed of the turbine (this is not surprising as in the standard control case the collective blade pitch is used to regulate the rotor speed). Thus, this collective loop is not used for load reduction, but instead for rotor speed control. In the case of IPC, the standard controller logic determines the behavior of the collective pitch angle, as if no individual pitch control actions were taking place. In the IFC case, the collective TEF deployment angle is an extra degree of freedom, which may be neglected by setting the value to zero at all times, or it can be used to augment rotor speed control by acting simultaneously with the standard controller collective pitch action. This possibility is discussed below.

2.2.3 Load Reduction Controller Architecture. By using the multiblade coordinate transformation, it is assumed that three independent, LTI SISO feedback loops result. LTI SISO systems are easily dealt with from a control perspective, as classical control techniques such as PID control can be employed. Once again, it is important to emphasize that only two feedback loops are needed to control the loads on all three blades. Thus, the control architecture used to reduce the loads on the blades is summarized as follows.

1. The blade root flapwise bending moments of the blades M_{y1} , M_{y2} , and M_{y3} are transformed into the fixed frame of reference using P^{-1} , yielding M_{y2}^{cm} and M_{y3}^{cm} , the hub yaw-wise and tiltwise moments, respectively.
2. The transformed loads M_{y2}^{cm} and M_{y3}^{cm} are used as inputs to a controller, and the control actions in the fixed frame θ_{y2}^{cm} and θ_{y3}^{cm} are calculated. The system is approximated as LTI in the fixed frame.
3. The control actions in the fixed frame θ_{y2}^{cm} and θ_{y3}^{cm} are transformed into the rotating frame using P . These are the demanded control actions of the TEFs or the blade pitch θ_1 , θ_2 , and θ_3 .

This approach can also be visualized using Fig. 1. A variety of control approaches are possible using this method of multiblade transformation. While PID controllers are easily implemented, more complex control approaches such as linear-quadratic-regulator (LQR) techniques can be used, and have been employed in the past [8,18]. The research presented here, however, is not focused on optimal control design. Rather, the goal is to design a “good” controller, which is easily implemented and that achieves sizable load reduction. Thus, PID control techniques are used exclusively, which have been shown to be nearly as effective as more complex LQR techniques anyway [18].

For IPC, Fig. 1, Eqs. (1) and (2) indicate that the individual blade pitch commands calculated for load reduction are superimposed on the collective blade pitch command utilized for rotor speed regulation. As stated above, the collective blade pitch control logic is unchanged from the standard controller case. Therefore, the collective blade pitch command is identical for the SC and IPC cases, with individual commands superimposed on the collective command in the IPC case.

Lastly, there is some debate about whether or not this pitch control approach is technically “individual pitch control” or “cyclic pitch control.” The authors are aware of this debate, and elect to use “individual pitch control” to describe the approach that is used. Because the blade loads are directly fed back to determine the blade pitch signal of each blade, instead of prescribing the pitch signal, we believe that this indicates an individual pitch control approach.

2.2.4 Controller Implementation. For the IFC case, the deployment range of the TEFs is limited to ± 10 deg, and the rate of change in the TEF deployment angle is limited to ± 40 deg/s. The TEFs are used for load reduction across all operating ranges, including regions 2 and 3.

The IPC controller is only utilized in the above rated conditions (region 3), similarly to collective pitch control. For both the collective pitch control in the standard controller case and the IPC case, the deployment range of the blade pitch is restricted to 0–90 deg, and the pitch rate is limited to ± 8 deg/s. The controller gains for IFC and IPC are detailed in the previous paper [1]; clearly the specific values of the gains are different for IFC and IPC, despite the identical controller structure.

As discussed previously, in the case of IFC, the collective TEF angle is an extra degree of freedom, unused for load reduction. This flexibility can be exploited by using the collective TEF angle to also help control the rotor speed for power regulation in region 3, in order to augment the collective pitch angle that is used for this purpose, and potentially result in smoother power production and less wear on the pitch system. Thus, a simple proportional controller (P only) is used to control the collective TEF angle, with the generator speed error used as the input signal to the controller. The collective TEF angle has a position limit of ± 5 deg, so as not to overwhelm the TEF deployment for load reduction (limited to ± 10 deg) when they are superimposed.

2.3 Simulation Run. Two categories of load cases are used to assess the performance of the various control approaches during these extreme events, and are summarized here. In order to isolate the effectiveness of IFC and IPC at reducing the damage caused by gusts and extreme loads, simple step increases in the wind speed are utilized in the two load cases. These step functions occur over some specified period of time, in the absence of wind shear, tower shadow, gravity loads, and turbulence. While these load cases are extremely simple, and not particularly realistic, they are effective at illuminating the underlying physical effects of gusts and the corresponding response of the various control approaches. By excluding other load sources such as wind shear, the loads due specifically to the gusts are not obscured. All simulations have a total length of 100 s, and in all cases the SC, IPC, and IFC approaches are used.

1. *Global step change, 15 m/s.* The wind speed is initially constant at 15 m/s across the entire rotor. At some specified time, the gust occurs, increasing the wind speed to 20 m/s across the entire rotor. Thus, this is a global step change, as the gust occurs uniformly over the entire rotor, and not at specific locations within the rotor face. In essence, this type of gust simulates a very large scale eddy, with a characteristic length scale on the order of the rotor diameter or larger. The step increase in the wind speed occurs over several lengths of time: 0.5 s, 1.5 s, 3.0 s, 5.0 s, 7.5 s, and 10 s. The global step changes are depicted in Fig. 2.
2. *Local step change, 15 m/s.* The wind speed is constant at 15

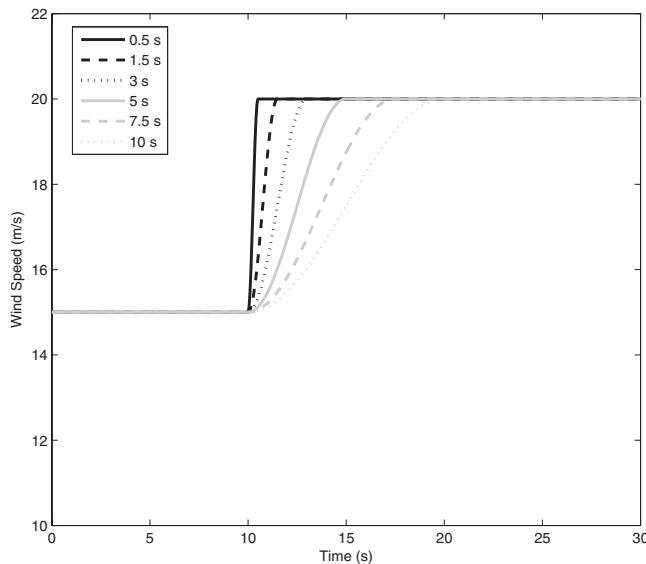


Fig. 2 Time series of hub height wind speeds for global step changes

m/s across the entire rotor, except for certain points within the rotor face where the wind speed is 20 m/s. A 13 point \times 13 point wind grid is used in these simulations. Only six points are potentially adjusted to values of 20 m/s, while the others always have values of 15 m/s. When looking at the rotor from upwind, these six points lie on the horizontal line at 3 o'clock, not including the center point of the grid. Figure 3 is useful for visualizing the situation. The 13 point \times 13 point grid is shown, along with a circle representing the rotor face. Three specific local step changes are considered. First, all six points on this line have values of 20 m/s. This encompasses the circle, square, and triangle points. Second, only the outer four points on the line have values of 20 m/s, and so only the square and triangle points. Finally, only the outer two points on the line have values of 20 m/s, and so only the triangle points. By adjusting these specific points in the wind input, a local gust is simulated. This ap-

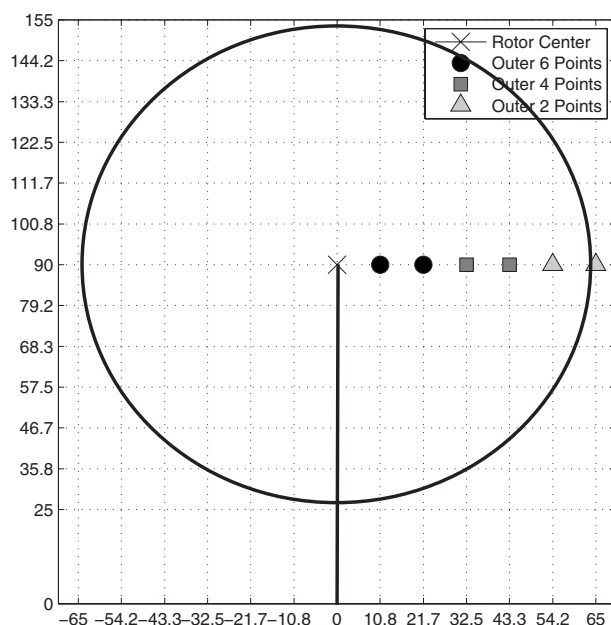


Fig. 3 Diagram of local step change gust locations

Table 1 Load reductions for global step change

Step length (s)	SC	IFC		IPC	
	$R(M_y)$ (N m $\times 10^6$)	$R(M_y)$ (N m $\times 10^6$)	Change (%)	$R(M_y)$ (N m $\times 10^6$)	Change (%)
0.5	6.91	6.76	-2.2	6.92	0.1
1.5	6.42	6.17	-4.0	6.44	0.3
3.0	5.46	5.11	-6.5	5.47	0.1
5.0	4.35	3.92	-9.7	4.36	0.3
7.5	4.03	3.69	-8.6	4.03	-0.2
10.0	3.48	3.22	-7.5	3.45	-1.0

proach allows for the effects of gusts at scales smaller than the rotor face to be examined.

3 Extreme Load Results and Discussion

The extreme load reductions are primarily calculated as the percent decrease in the range of the blade root flapwise bending moment M_y , where the range is calculated as the difference between the maximum and minimum values of M_y . The range of M_y is labeled $R(M_y)$. In reality, the maximum and minimum of M_y should be used separately to assess damage, not the range. In practice, for all cases considered in this research, when $R(M_y)$ is reduced, the maximum load is reduced and the minimum load is increased, and so using $R(M_y)$ simply condenses the results somewhat. It should be emphasized that the global step change and the local step change simulations both assume quasisteady aerodynamic behavior. This is a potentially erroneous assumption, and it is evaluated later.

3.1 Global Step Change. The values of $R(M_y)$ for the various control approaches and global step change lengths are shown in Table 1. The percent difference in $R(M_y)$ when using either IFC or IPC is also calculated and shown in Table 1. Table 1 indicates the following.

- IFC is effective at reducing $R(M_y)$ for all gust lengths. Specifically, $R(M_y)$ is decreased only slightly for very rapid gusts, i.e., gust lengths of 0.5 s and 1.5 s. For less rapid gusts occurring over 3 s or longer, the reductions in $R(M_y)$ are significant, with an average value of approximately 8%. This improved performance for longer gust lengths is explained below.
- It appears that IPC has a negligible effect on $R(M_y)$ for all gust lengths. A physical explanation for these results is presented below as well.
- Once again, it is important to note that the simulations operate under the assumption of quasisteady aerodynamic behavior. The rapid change in the wind speed during these simulations leads to unsteady aerodynamic effects.

Figure 4 shows the time series of M_y for blade 1 for all three control approaches (SC, IFC, and IPC), the blade pitch for the SC and IPC cases, and the TEF behavior for the IFC case. The time series are shown for both the 1.5 s gust length and the 5 s gust length. The gusts all begin 10 s into the simulation. Figure 4 indicates the following.

- M_y and the blade pitch are virtually identical for the SC and IPC cases, and, in fact, are indistinguishable in Fig. 4; i.e., the black and dashed gray lines are exactly on top of each other. This confirms the negligible change in $R(M_y)$, as shown in Table 1. Clearly, despite the rapid change in the wind speed and the blade loads, the blade pitch does not respond to reduce M_y in the IPC case.
- On the other hand, for both SC and IPC, the blade pitch does increase during the gust (it also increases in the IFC

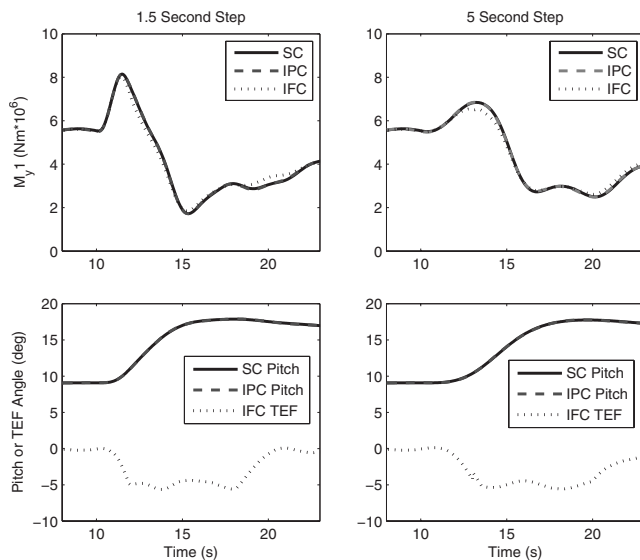


Fig. 4 Global step change time series results

case, which is not shown). This increase is a result of using the collective pitch angle for rotor speed control in above rated conditions. As the wind speed increases during the gust, the rotor speed increases, and so the collective pitch angle is also increased to reduce the aerodynamic torque on the rotor and reduce the speed to the rated value.

- For both gusts, IFC does, in fact, reduce the peaks in the M_y signal. The reduction is noticeably larger for the 5 s gust.
- During the gust, and for some time after the gust has finished, the TEF deflection is approximately constant at -5 deg. For the rest of the simulations, the TEF deflection is approximately 0 deg. In fact, the TEF behavior mirrors the blade pitch behavior: The collective TEF deflection is being used to control the rotor speed during the gusts. As described previously, when using IFC, the TEFs are also utilized to control the rotor speed in above rated conditions, and the collective TEF deflection angle is limited to ± 5 deg. Thus, since the gust causes the rotor speed to increase, the TEFs collectively deploy to a negative value to help slow the rotor down. Moreover, this indicates that the TEFs are not behaving so as to explicitly reduce the loads on the blades.

These results lead to an important conclusion regarding both IFC and IPC: During these types of gusts, despite the substantial changes in the blade loads (M_y), neither the TEFs nor the blade pitch explicitly respond to reduce the loads. This result initially appears curious, but, in fact, it is a direct function of two factors: the control architecture that is employed and the nature of the gusts that are utilized.

1. The blade root flapwise bending moments are transformed into nonrotating coordinates using the Coleman matrix, which then yields the tilt and yaw moments on the fixed rotor hub. For both IFC and IPC, the response of either the TEFs or the blade pitch aims to minimize these tilt and yaw moments. As the results of the fatigue load simulations indicate [1], this is an effective approach for reducing the blade fatigue loads. However, it must be emphasized that the explicit objective of this particular control architecture is not to reduce the blade fatigue loads directly, but instead to minimize the tilt and yaw moments, which then leads to reduced blade fatigue loads in most cases.
2. The gusts used in these simulations are “global” gusts, as the wind speed is uniform across the rotor face. As such, this type of gust does not generate a sizable tilt or yaw moment

on the rotor hub. The forces increase approximately equally on each blade, and so while the bending moments at the blade roots increase, the tilt and yaw moments do not increase appreciably when the gust is this global type.

When these two factors are considered together, it becomes clear why neither IFC nor IPC react to reduce the blade loads. A global gust, which is uniform across the rotor face, generates a very little tilt or yaw moment on the rotor hub, and so for the control architecture employed in this research, the TEFs or the blade pitch do not respond to reduce the blade loads.

The decrease in $R(M_y)$ that occurs in the IFC simulations is a result of using the collective TEF deployment for controlling the rotor speed in above rated conditions. The resulting decrease in the blade loads is an ancillary benefit of this use of the TEFs; it is not the explicit goal of using the collective TEFs but instead is a secondary effect. This reduction in $R(M_y)$ should not be discounted, however. A substantial reduction in the blade loads is possible during these global gusts as long as the collective TEF deployment is utilized for controlling the rotor speed. It is also now clear why the load reductions are larger for the 5 s gust than the 1.5 s gust. For the faster 1.5 s gust, the TEFs are not fully deployed collectively to -5 deg until approximately 2 s after the gust begins, and so the loads are not significantly reduced during the gust itself. Essentially, the gust occurs so quickly that by the time the TEFs are collectively deployed to control the rotor speed, the transient portion of the gust has finished. For the 5 s gust, the TEFs are fully deployed collectively to -5 deg approximately 3 s after the gust begins, and so they are able to affect the loads during the gust itself. The result is that the peak of M_y is reduced appreciably during this slower gust.

In all cases, SC, IPC, or IFC, $R(M_y)$ can be reduced by increasing the rate of response of the collective blade pitch control, by both changing the controller gains for the collective blade pitch control, and increasing the blade pitch rate limit. These changes would allow the blade pitch to respond more rapidly to the global gusts, and so reduce $R(M_y)$. The drawbacks to such changes are twofold. First, by changing the collective pitch controller gains, the blade pitch behavior at other operating points, such as during normal turbulent wind, is changed, and these gains were tuned originally to give good performance at these operating points. It is likely that during normal turbulent wind operation, the pitch usage would increase substantially if the gains are tuned to give a faster response during gusts. Second, increasing the pitch rate limits will result in an even greater demand on the pitch drive system in some situations, and so there will be greater fatigue of some components. These potential changes are outside of the scope of this paper. Moreover, given that the vast majority of the operation of a wind turbine is not during large scale gusts, it seems unlikely that one would tune the collective pitch controller for these specific situations.

Overall, these results help highlight some of the limitations of the control architecture that is utilized in this research. Specifically, the explicit goal of the controller is not blade fatigue load reduction, but instead it is minimization of the tilt and yaw moment on the rotor hub. While this goal leads to reduced blade fatigue loads the majority of the time, there are also instances, such as gusts with spatial scales on the order of the rotor diameter or larger, in which the control architecture is ineffective. Other control approaches, perhaps those that utilize the measured blade loads directly, or those that also attempt to add damping to the tower fore-aft motion, may be more effective during these large scale gusts.

It should be noted that in below rated conditions, during global gusts, IFC would be equally ineffective compared with the SC and IPC approaches. That is, in below rated conditions, the collective TEF deployment angle is not utilized, and so the blade loads are unchanged compared with SC, because the global gust generates a very little tilt or yaw moment. On the other hand, it is debatable if

Table 2 Load reductions for local step change

No. of local wind grid points	IFC	IPC
	Change (%)	Change (%)
2	-15.4	0.1
4	-15.0	-8.7
6	-15.2	-10.5

it would even be desirable to reduce the blade loads during gusts in below rated conditions. When a gust occurs, the rotor speeds up to capture as much energy from the wind as possible. If the TEFs were deployed to reduce the loads on the blades during gusts, they would also act to retard the increase in rotor speed, and therefore reduce the power extracted from the wind.

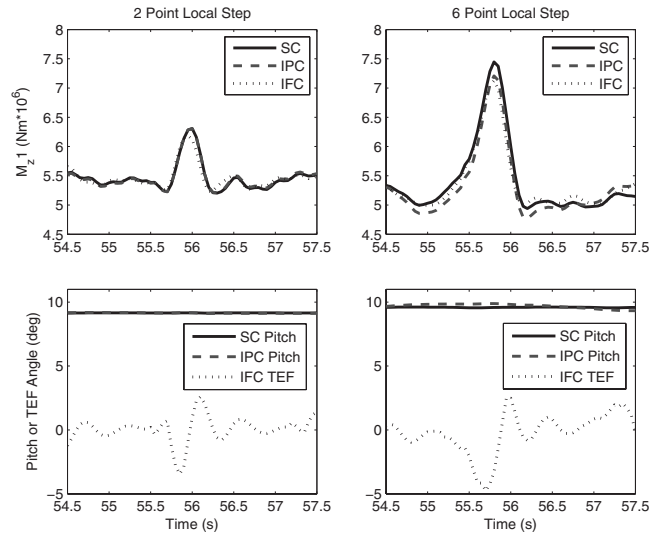
Finally, any type of gust that is uniform across the rotor face is likely to produce similar results. The IEC-type gusts are no exception, as all uniform gusts do not produce sizable tilt or yaw moments, and therefore no explicit load reduction action takes place.

3.2 Local Step Change. For the local step change simulations, each time the blade passes through the localized region of higher wind speed, it experiences a gust. As such, for a 100 s simulation, each blade will experience this local gust 20 times. The results are consolidated as follows. First, the maximum value of M_y is determined each time the local gust occurs, yielding 20 values. Next, the difference between each maximum value and the average value of M_y during the entire simulation is calculated. Finally, the average for the 20 differences is computed. In sum, the average difference between the maximum value of M_y during each gust and the average value of M_y during the entire simulation is calculated. This is essentially a calculation of the average value of $R(M_y)$ for each gust, except that the average value of M_y is used instead of the minimum value. The average value is used because it is constant for each control approach utilized, whereas the minimum value differs somewhat. In general, however, the difference is small, and the distinction is made here only for completeness. $R(M_y)$ is used to label the results once again, even though it is calculated differently.

The values of the percent difference in $R(M_y)$ when using either IFC or IPC is calculated for the number of altered wind grid points and shown in Table 2. Table 2 indicates the following.

- For all three local gusts, IFC results in substantial reductions in $R(M_y)$. The reductions in $R(M_y)$ are essentially constant at approximately 15%.
- For IPC, $R(M_y)$ is reduced sizably when six points of the wind grid are altered (although not as much as IFC), but the ability to reduce $R(M_y)$ worsens as the number of altered points is reduced.
- Once again, it is important to note that the simulations operate under the assumption of quasisteady aerodynamic behavior. The rapid change in the wind speed during these simulations leads to aerodynamic behavior that is not quasisteady.

These results clearly indicate an important distinction between IFC and IPC, namely, the bandwidth of the two load control approaches. As the number of altered points in the wind grid is decreased, the scale of the local gust is decreased as well. Moreover, the effects of the gust are felt by the blade over a shorter period of time. When all six points in the wind grid are altered, a passing blade is affected by the gust for approximately 2.5 s. In the case of four altered points, this value is reduced to approximately 0.8 s, and for two altered points it is only approximately 0.4 s. Because IFC has significantly higher bandwidth than IPC,

**Fig. 5 Local step change time series results**

the ability to reduce the local gusts appears to be independent of the scale of the local gust. In contrast, the effectiveness of IPC is highly dependent on the scale of the local gust. Overall, these results indicate a clear advantage of using IFC compared with IPC.

The distinction between these local gusts and the global gusts discussed above should also be emphasized. The global gusts are uniform across the rotor face, and therefore produce very little changes in the tilt and yaw moments on the rotor. In contrast, the local gusts, which occur solely on one blade, do indeed produce a yaw or tilt moment. For the specific location of the local gusts used in these simulations, a yaw moment is produced. More generally, a local gust produced on a blade must generate a tilt or yaw moment, and so the load control approaches, whether IFC or IPC, indeed react and reduce the blade loads.

Figure 5 shows a 3 s window of the time series of M_y for blade 1 for all three control approaches (SC, IFC, and IPC), the blade pitch for the SC and IPC cases, and the TEF behavior for the IFC case. The time series are shown for the cases when two and six local wind data points are altered. Figure 5 indicates the following.

- The length of time that the blade is affected by the local gust is clearly highlighted, as the gust when only two points are altered occurs over a significantly shorter period of time than when six points are altered. As a result, the loads are increased more when six points are altered, as the blade has a longer time to feel the effect of the increased wind speed.
- The TEFs behave similarly for either IFC simulation, and clearly act to reduce the loads on the blades during the local gust. The range of deployment is fairly small, approximately ± 3 deg. This response of course depends on the gains used for the controller.
- For IPC, the blade pitch has a negligible reaction when two local points are altered, and a very small reaction when six points are altered. The slow reaction of the blade pitch is clearly highlighted in these time series.

In sum, when local gusts on the scale of the blade or smaller occur, the load control approaches display vastly different behaviors and effectiveness. The significantly higher bandwidth of IFC appears to be a valuable asset during these local gusts, and an important advantage relative to IPC.

4 Limitations of Results

The BLADED simulations rely on a number of assumptions, and it is important to justify some of these to help establish the valid-

ity of the results. In particular, the assumption of quasisteady aerodynamics is now assessed. The use of TEFs is mutually exclusive with the dynamic stall model implemented in BLADED, and so unsteady aerodynamic effects are suppressed.

The assumption of quasisteady aerodynamic behavior implies that during operation, as the angle of attack of an airfoil section changes and as the TEF deflects to control loads, the aerodynamic performance of the airfoil, characterized by C_L , C_D , and C_M , is determined directly from the airfoil tables that are inputted into BLADED. Thus, the aerodynamic performance is calculated in a quasisteady manner, by assuming that C_L , C_D , and C_M change with each time step dependent solely on the values of α and the TEF deployment angle (for the TEF sections), and not on how quickly these parameters change.

In reality, the aerodynamic performance of the airfoil sections responds to changes in α and the TEF deployment angle in a dynamic sense. A rapid change in the angle of attack does not result in an instantaneous change in C_L , C_D , and C_M ; instead, C_L , C_D , and C_M change over some period of time until they reach a steady state value. Only when the angle of attack and the TEF deployment angle change slowly enough is the assumption of quasisteady aerodynamics a valid approximation. Leishman [19] provided a detailed look at unsteady aerodynamic behavior for a rotor. Gaunaa [20] and Hansen et al. [21] investigated unsteady aerodynamic effects for blades with deformable trailing edge geometry (DTEG), and developed unsteady and dynamic stall models for these sections. The models are used by Anderson et al. [7,22] in their simulations of smart blades.

The issue of unsteady aerodynamics is particularly important in the context of smart rotor control. For very rapid changes in the inflow conditions, and therefore in the loads, there is a phase delay between the actual disturbance and the aerodynamic response of the airfoil section, and so the loads. Since the load reduction controllers, using IFC or IPC, respond to the measured blade loads, the response of the controllers is therefore delayed when the disturbance occurs very rapidly, and so the load mitigation abilities are reduced.

When an airfoil section experiences some disturbance, the degree of unsteadiness caused by that disturbance can be quantified by the reduced frequency, k . k is a nondimensional parameter, and is determined using Eq. (3), where c is the local chord length of the section, U is the local relative velocity at the section, and ω is the frequency of the disturbance, in units of rad/s [19].

$$k = \frac{c}{2U} \omega \quad (3)$$

The larger the value of k , the more the actual performance of the airfoil deviates from the performance when one assumes quasisteady behavior. As a general rule, when $k < 0.05$, the aerodynamics can be considered quasisteady, and when $k > 0.05$ they are considered unsteady.

The extreme load simulations are analyzed to assess the possible effects of assuming quasisteady aerodynamic behavior. For each global gust, a simple analytic method is utilized to quantify the degree of unsteadiness in the simulations, and approximate the reduced frequency. The global gusts are shaped similarly to the first quarter of a sine wave, i.e., the first 90 deg. The TEF behavior during the global gust shows a similar shape, as does the angle of attack. It is therefore assumed that the global gust represents the first fourth of a sinusoidal variation in the wind speed, the TEF deflection, and the angle of attack. As such, the frequency ω , used to calculate k in Eq. (3), is simply the inverse of four times the global step length. So, for a 0.5 s gust, the period of the disturbance is assumed to be 2 s, and so the frequency is 0.5 Hz or 3.14 rad/s. For a 10 s gust, the frequency is only 0.157 rad/s. Next, k is calculated for the blade station $r=52.75$ m, with $c=2.518$ m and U taken as the average relative wind speed during the simulation,

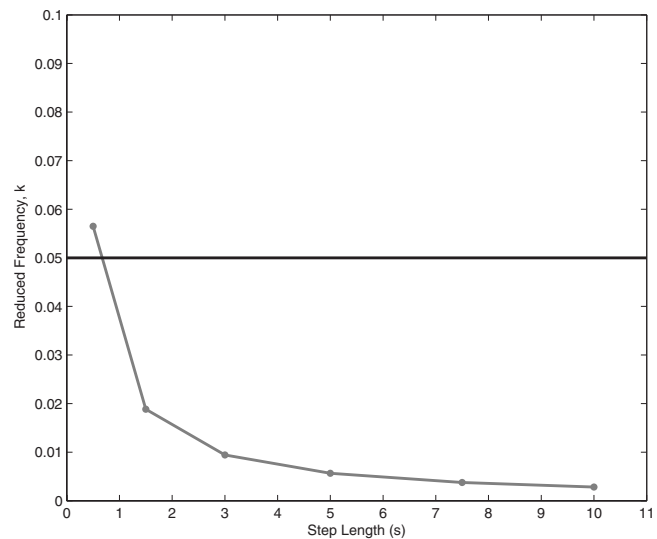


Fig. 6 Evaluation of unsteadiness for global gust

which is approximately 70 m/s in every case. The results are shown in Fig. 6, which shows the computed values of k as a function of the global step length.

Figure 6 clearly indicates that k decreases as the global step length increases. This is logical, as a slower gust should indeed result in a behavior that is closer to quasisteady than a faster gust. Moreover, with the exception of the 0.5 s step length, k is less than 0.05 in all cases, and therefore these instances appear to be quasisteady in nature. Even for the 0.5 s step, the value of k is approximately 0.057, and so it is only slightly greater than 0.05. Thus, with the exception of the 0.5 s step change in the wind speed, the results of the global gust simulations appear to be such that assuming quasisteady aerodynamic behavior is indeed a valid assumption, and so the results can be trusted for the TEF section. Again, this is a simple and approximate approach to evaluating the unsteadiness of the aerodynamics, but it does help indicate whether or not the assumption of quasisteadiness is valid.

The local gusts are evaluated as well, to determine the validity of the assumption of quasisteady aerodynamic behavior. The reduced frequency is approximated in a similar manner as the global gusts. For the local gusts, the time series indicate that TEF deflection angle executes essentially one full cycle during each local gust. That is, the TEF deflection resembles a sine wave during each local gust, and so does the angle of attack. Thus, the period of each local gust is used to calculate the frequency of the disturbance and therefore the reduced frequency k . As with the global gust, k is calculated for the blade station $r=52.75$ m, with $c=2.518$ m and U taken as the average relative wind speed during the simulation, which is approximately 69 m/s in every case. The results are shown in Fig. 7, which shows k as a function of the number of altered wind grid points.

Figure 7 indicates that using this method to estimate the unsteadiness of the gust results in potentially very large values of k . In fact, only in the case where six of the wind grid points are altered, which is a larger spatial gust, is the value of k less than 0.05. For the other two cases, k is significantly larger than 0.05, indicating a highly unsteady situation. While this method for calculating k is simple and approximate, it appears to indicate that the results may be invalid when only two or four wind grid points are altered. On the other hand, the results when six wind grid points are altered appear to be valid, and the conclusions drawn from these results are likely sound. Namely, IFC is more effective at reducing the effects of small scale gusts, with characteristic length scales on the order of the blade length or less.

Finally it should be noted that for all evaluations of unsteadiness, the degree of unsteadiness depends strongly on the spanwise

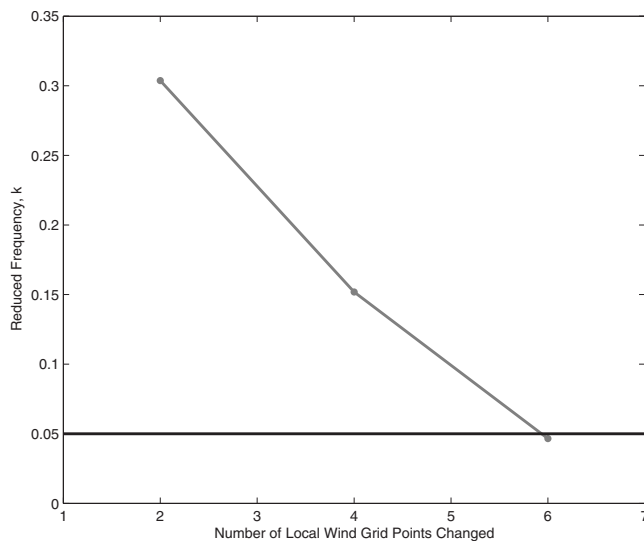


Fig. 7 Evaluation of unsteadiness for local gust

blade section under consideration. The inboard sections, where the chord length is larger and the relative wind speed is smaller, have larger reduced frequencies. This is a difficult issue to assess comprehensively. On one hand, there are no TEFs on these inboard sections, and so any errors due to unsteady aerodynamic effects will be constant across all the simulations. It is only on the TEF section where the simulations may differ in terms of unsteady aerodynamic behavior. On the other hand, the assumption of quasisteadiness along the entire blade calls into question the validity of the results for all blade sections and all simulations, whether or not TEFs are modeled, and especially near the root section where k is larger. While it is outside the scope of this paper to fully assess this issue for aero-elastic simulations of wind turbine blades, one recommendation appears certain: Unsteady aerodynamic and dynamic stall models specifically for TEF sections should be developed and implemented into aero-elastic simulations, so that these effects can be modeled not just on the TEF section but also along the entire blade.

5 Conclusions

The primary goal of smart rotor control is to reduce fatigue loads on the blades, and the controller used in this research is designed for this purpose. However, extreme loads caused by gusts and other transient operations also cause damage in wind turbines, and it is important to determine if smart rotor control approaches can be effective during these situations as well. This research investigates the performance of smart rotor control approaches, designed for fatigue load reduction, during extreme load events. The major conclusions of this research are as follows.

- The control approach utilized for fatigue load reductions, namely, the multiblade transformation, is ineffectual at reducing the blade loads during large scale global gusts. These gusts do not produce sizable yaw or tilt moments, and so the response of IFC or IPC is minimal.
- The use of the trailing edge flaps for rotor speed control in above rated conditions has the ancillary benefit of reducing blade loads due to global gusts. This is a secondary effect, but valuable nonetheless, and explains the reduced loads in the IFC cases for the global gusts.
- For small scale gusts, the significantly higher bandwidth of TEFs results in superior load reduction compared with IPC.
- Unsteady aerodynamics are important effects during gusts, and the degree of unsteadiness in a simulation should be assessed. While most results from the simulations appear valid, some should be qualified due to large reduced frequencies. Specifically, the local gusts results when only two

or four points are altered have large reduced frequencies and so may not be valid. More broadly, the need for unsteady aerodynamic and dynamic stall models specifically for TEF sections is clear, and these should be implemented into aero-elastic codes, so these effects can be modeled on all blade sections.

Acknowledgment

The authors would like to acknowledge STW for funding this research, and Ervin Bossayni, Thanasis Barlas, and Jan-Willem van Wingerden for their contributions.

Nomenclature

- C_D = coefficient of drag
 C_L = coefficient of lift
 C_M = coefficient of pitching moment
IEC = International Electrotechnical Commission
 k = reduced frequency
LTI = linear time invariant
 M_y = blade root flapwise bending moment
SC = standard control
 α = angle of attack

References

- [1] Lackner, M., and van Kuik, G., 2009, "A Comparison of Smart Rotor Control Approaches Using Trailing Edge Flaps and Individual Pitch Control," 47th AIAA Aerospace Science Meeting and Exhibit.
- [2] Barlas, T., 2006, "Smart Rotor Blades and Rotor Control for Wind Turbines: State of the Art," knowledge base report for upwind wp 1b3, Delft University Wind Energy Research Institute (DUWIND), Report No. UpWind WP 1B3.
- [3] Barlas, T., and van Kuik, G., 2007, "State of the Art and Prospectives of Smart Rotor Control for Wind Turbines," J. Phys.: Conf. Ser., **75**, p. 012080.
- [4] van Engelen, T., and van der Hooft, E., 2005, "Individual Pitch Control Inventory," Technical University of Delft, Technical Report No. ECN-C-03-138.
- [5] Bossayni, E., 2003, "Individual Blade Pitch Control for Load Reduction," Wind Energy, **6**, pp. 119–128.
- [6] Selvam, K., 2007, "Individual Pitch Control for Large Scale Wind Turbine," MS thesis, Technical University of Delft, Delft, The Netherlands.
- [7] Andersen, P., Henriksen, L., Gaunaa, M., Bak, C., and Buhl, T., 2008, "Integrating Deformable Trailing Edge Geometry in Modern Mega-Watt Wind Turbine Controllers," 2008 European Wind Energy Conference and Exhibition.
- [8] McCoy, T., and Griffin, D., 2006, "Active Control of Rotor Aerodynamics and Geometry: Status, Methods, and Preliminary Results," 44th AIAA Aerospace Science Meeting and Exhibit.
- [9] Lackner, M., and van Kuik, G., 2009, "A Comparison of Smart Rotor Control Approaches Using Trailing Edge Flaps and Individual Pitch Control," Wind Energy, to be published.
- [10] Zayas, J., van Dam, C., Chow, R., Baker, J., and Mayda, E., 2006, "Active Aerodynamics Load Control for Wind Turbine Blades," European Wind Energy Conference.
- [11] Bossayni, E., 2003, GH BLADED Version 3.80 Theory Manual, Garrad Hassan and Partners.
- [12] Bossayni, E., 2004, GH BLADED Version 3.80 User Manual, Garrad Hassan and Partners.
- [13] Jonkman, J., Butterfield, S., Musial, W., and Scott, G., 2008, "Definition of a 5-MW Reference Wind Turbine for Offshore System Development," National Renewable Energy Laboratory Report No. TP 500-38060.
- [14] Trolborg, N., 2005, "Computational Study of the Risøb1-18 Airfoil With a Hinged Flap Providing Variable Trailing Edge Geometry," Wind Eng., **29**(2), pp. 89–113.
- [15] Drela, M., and Youngren, H., 2001, XFOIL 6.9 User Primer, MIT.
- [16] Bir, G., 2008, "Multi-Blade Coordinate Transformation and Its Application to Wind Turbine Analysis," 46th AIAA Aerospace Science Meeting and Exhibit.
- [17] Coleman, R., and Feingold, A., 1958, "Theory of Self-Excited Mechanical Oscillations of Helicopter Rotors With Hinged Blades," NASA, Technical Report No. 1351.
- [18] Bossayni, E., 2004, "Developments in Individual Pitch Control," EWEA Special Topic Conference: The Science of Making Torque From Wind.
- [19] Leishman, J., 2006, *Principles of Helicopter Aerodynamics*, Cambridge University Press, Cambridge.
- [20] Gaunaa, M., 2005, "Unsteady 2D Potential-Flow Forces on a Variable Geometry Airfoil Undergoing Arbitrary Motion," Risø, Technical Report No. R-1478(EN).
- [21] Hansen, M., Gaunaa, M., and Madsen, H., 2004, "A Beddoes-Leishman Type Dynamic Stall Model in State-Space and Indicial Formulations," Risø, Technical Report No. R-1354(EN).
- [22] Andersen, P., Gaunaa, M., Bak, C., and Buhl, T., 2006, "Load Alleviation on Wind Turbine Blades Using Variable Airfoil Geometry," 2006 European Wind Energy Conference and Exhibition.